The Canadian Mineralogist
Vol. 52, pp. 501-511 (2014)
DOI: 10.3749/canmin.52.3.501

PERMINGEATITE, Cu_3SbSe_4, FROM PŘÍBRAM (CZECH REPUBLIC): DESCRIPTION AND RAMAN SPECTROSCOPY INVESTIGATIONS OF THE LUZONITE-SUBGROUP OF MINERALS

PAVEL ŠKÁCHA[§]

Institute of Geochemistry, Mineralogy and Mineral Resources, Charles University in Prague, Faculty of Science, Albertov 6, CZ–128 43, Praha 2, Czech Republic

Mining Museum Příbram, Hynka Kličky Place 293, 261 01, Příbram VI - Březové Hory, Czech Republic

ELENA BUIXADERAS

Department of Dielectrics, Institute of Physics, ASCR v.v.i., Na Slovance 2, 182 21 Prague 8, Czech Republic

JAKUB PLÁŠIL

Department of Structure Analysis, Institute of Physics, ASCR v.v.i., Na Slovance 2, 182 21 Prague 8, Czech Republic

JIŘÍ SEJKORA

Department of Mineralogy and Petrology, National Museum, Cirkusová 1740, CZ–193 00, Praha 9, Czech Republic

VIKTOR GOLIÁŠ

Institute of Geochemistry, Mineralogy and Mineral Resources, Charles University in Prague, Faculty of Science, Albertov 6, CZ–128 43, Praha 2, Czech Republic

VOJTĚCH VLČEK

Bayerisches Geoinstitut, Universität Bayreuth, Universitätsstraße 30, D-95447 Bayreuth, Germany

ABSTRACT

Permingeatite from a new occurrence, the Příbram uranium-base metal ore district (central Bohemia, Czech Republic), has been studied in detail. Its occurrence is similar to the type occurrence in Předbořice (Czech Republic). Based on electron microprobe analysis, the empirical formula of the studied permingeatite (mean of 10 point analyses, based on Sb + Cu + Fe + Se + S = 8 *apfu*) is $Cu_{3.00}(Sb_{0.99}Fe_{0.04})_{\Sigma 1.03}(Se_{3.74}S_{0.23})_{\Sigma 3.97}$. The unit-cell parameters refined from powder X-ray diffraction data are *a* 5.6323(2) Å, *c* 11.2354(7) Å, with *V* 356.41(2) Å^3 (for space group $I\bar{4}2m$). The Se-S substitution is characteristic for the permingeatite from Příbram, in contrast to permingeatite from Předbořice, where the As-Sb substitution dominates. Regarding substitution trends, only two, Sb-As and S-Se, play a role in the luzonite group minerals. The only other element (as documented by the present study) which enters the structure of the luzonite-group minerals in considerable concentrations is Fe. Raman spectroscopy was used to characterize vibrational properties of the luzonite group of minerals. The dominant feature in the Raman spectra of the studied minerals is a suite of spectral bands that corresponds to the stretching and bending vibrations of tetrahedral XY_4 (X = As/Sb; Y = S/Se) groups. Intrinsic shifts in observed energies for distinct studied minerals are connected with different elemental compositions of the tetrahedral groups. The reflectance data obtained from the studied permingeatite are close to the published data, but more significant differences were found, particularly in the areas of 420–500 nm and about 640 nm. The studied association was formed, based on the presence of umangite, at temperatures below 112 °C.

Keywords: permingeatite, luzonite subgroup, Raman spectroscopy, reflectance, selenide minerals, Příbram, Czech Republic

§ *Corresponding author e-mail address:* skachap@seznam.cz

Introduction

Permingeatite was originally described as a new mineral species from the Předbořice uranium deposit (Czech Republic) by Johan *et al*. (1971). It is a member of the luzonite subgroup of the stannite group, along with luzonite, Cu_3AsS_4 (Weisbach 1874), and famatinite, Cu_3SbS_4 (Stelzner 1873). All three are isostructural, crystallizing in the space group $I\bar{4}2m$ with a derivative of the sphalerite structure. Enargite is an orthorhombic analogue of luzonite with a wurtzite-type structure (Pauling & Weinbaum 1934). The Se-analogue of both luzonite and enargite is not known. The complete solid-solution series between luzonite and famatinite was discovered by Pfitzner & Bernert (2004). There are a few investigations of crystal structures and phases of the famatinite-luzonite series, primarily carried out on synthetic compounds (Pfitzner 1994, Pfitzner & Reiser 2002, Pósfai & Buseck 1998), but also of natural materials (Gaines 1957, Marumo & Nowacki 1967).

The current study aims to present new experimental data for natural permingeatite, obtained using specimens from the uranium-base-metal district near Příbram (central Bohemia, Czech Republic) (Fig. 1). Permingeatite is an extremely rare Se mineral found only in uranium deposits in the Czech Republic and mostly with microscopic dimensions. We used the opportunity to study rare macroscopic permingeatite by electron microprobe, reflectance, powder X-ray diffraction, and Raman spectroscopy. The newly obtained results are compared here with those previously published, and are further discussed in broader relation to the luzonite subgroup of minerals. This paper is part of our systematic study of selenides from various types of Czech occurrences (Litochleb *et al*. 2004, Sejkora *et al*. 2006, 2011, Škácha *et al*. 2009a,b, 2010, Topa *et al*. 2010) in order to better understand the evolution of Se-mineralization in similar camps.

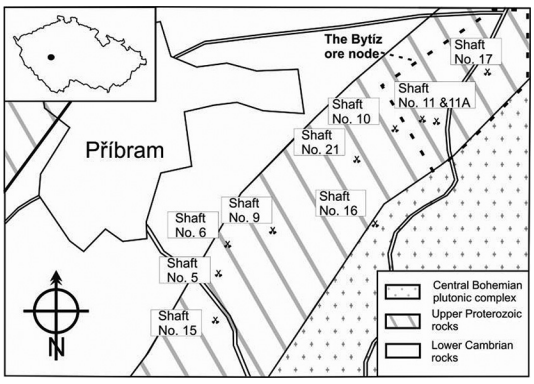

FIG. 1. Simplified geological map of the Příbram area.

Geology and Mineralogy

A new occurrence of the rare species permingeatite, Cu_3SbSe_4, has been discovered in the uranium and base-metal district near Příbram, Central Bohemia, Czech Republic, where specimens with permingeatite were found in dump material from the "No. 11A" (Bytíz) uranium mine. This uranium and base-metal district is situated in an exocontact of the Central Bohemian plutonic complex with the Teplá-Barrandien sedimentary unit. Uranium mineralization occurs in a zone 25 km in length and up to 2 km wide. The hydrothermal ore veins are concentrated in so called "ore nodes". Shaft No. 11A is located in the most important "Bytíz ore node", in the central part of the district. In the "Bytíz ore node" significant uranium reserves were located in veins Bt4 and Bt4H, with totals of 3673 and 1810 t of mined U. This ore node overall provided 52% of the production of the entire Příbram uranium district. Shaft 11A exposed the upper parts of the veins from the surface to a depth of 1500 m. The underground mining of uranium in Příbram area took place from 1948 to 1991 (Ettler *et al*. 2010).

There are four main mineralization stages in the Příbram deposit: (1) siderite-sulphidic; (2) calcite; (3) calcite-uraninite; and (4) calcite-sulphidic. Selenides are closely related to uraninite in carbonate veins within the third mineralization stage. Uranium ore is represented by dominant uraninite (pitchblende form), coffinite, and "antraxolite". Uraninite dating by U-Pb gave an age of 265 ± 15 Ma (Legierski 1973). Uraninite from the nearby Příbram base-metal deposit has similar ages (269.8 ± 20.3 Ma and 263.2 ± 8.9 Ma) (Škácha *et al*. 2009a). Selenium mineralization is relatively rare at Příbram and was first mentioned by Růžička (1986) and more recently by Litochleb *et al*. (2004), who recognized an assemblage of selenides on a historical specimen from the 1950's in the National museum's collection (Prague, Czech Republic). Large amounts of selenides were recently found in dump material from shafts no. 11A Bytíz and no. 16 Háje (Škácha *et al*. 2009a,b, 2010). We suggest that the majority of this material originated from the Bt4 vein, because this vein was the most important vein in the deposit, accounting for the majority of mined material with uranium ores. The Příbram carbonate veins containing uraninite originated from low-temperature (80–140 °C) and low-salinity fluids, according to the fluid inclusion study (Žák & Dobeš 1991). The origin of selenides in carbonate veins follows the crystallization of uraninite, as the redox potential of the hydrothermal fluids fell and the fugacity of Se increased (Dymkov 1985).

Description of the Sample

The permingeatite-bearing specimen analyzed in this study, originally about 15 × 10 × 10 cm in size, is made up of a complicated system of calcite veins of 1

cm average thickness, maximally about 2 cm. Calcite is strongly hematitized at the edges, and is rarely milky white, but more often black due to numerous inclusions of selenides and sulphides, at the cores. Local country rock has been strongly hematitized.

Permingeatite is found rarely as large irregular grains up to 1 mm in size, growing in groups in brownish or blackish younger carbonate (mostly calcite) veins in association with chalcopyrite, hematite, uraninite, löllingite, clausthalite, hakite, berzelianite, umangite, and eskebornite. It forms compact intergrowths with hakite and eskebornite. Permingeatite grains frequently have thin rims of clausthalite (Fig. 2). Fine-grained aggregates of permingeatite are macroscopically bronze brown in color with a yellowish tint, showing strong metallic luster. Uraninite is locally abundant on the specimen occurring in kidney-shaped black aggregates with strong glassy luster.

Experimental

Quantitative chemical data for the studied samples were obtained using a Cameca SX100 electron microprobe (at the Laboratory of Electron Microscopy and Microanalysis of Masaryk University and Czech Geological Survey, Brno) in the wavelength-dispersive mode with an accelerating voltage of 25 kV, a specimen current of 20 nA, and a beam diameter of about 1 μm. The following standards and X-ray lines were used: Cu (Cu$K\alpha$), Ag (Ag$L\alpha$), PbSe (Se$L\beta$), $CuFeS_2$ (S$K\alpha$), CdTe (Cd$L\beta$), PbS (Pb$M\alpha$), Sb (Sb$L\beta$), and Bi (Bi$M\beta$). Peak counting times (CT) were 20 s for all elements, and CT for the background was one half that of the peak time. Raw intensities were converted to concentrations using PAP (Pouchou & Pichoir 1985) matrix-correction software.

X-ray powder diffraction data were collected with a PANalytical X'Pert Pro powder diffractometer equipped with an X'Celerator solid-state detector and a secondary graphite monochromator using Cu$K\alpha_{1,2}$ radiation (40 kV and 30 mA). Data were measured over the range between 10 and 100° 2θ with 0.02° step size and a counting time of 10 s per step. Peak positions and intensities were determined using the XFIT program using the Pearson VII profile function (Coelho & Cheary 1997). Relative intensities were obtained with the High-Score program (PANalytical 2003). The unit-cell parameters of permingeatite were refined from the powder X-ray diffraction data using the UnitCell software (Holland & Redfern 1997).

A Renishaw RM-1000 Raman microscope was used to collect Raman spectra from separated permingeatite grains mounted in a polished section. Raman scattering was excited with an Ar laser of wavelength 514.5 nm operating at a power of 6 mW (about 1 mW on the sample) and spectra were recorded in backscattering geometry. The frequency calibration was done on Si wafer. The estimated diameter of the laser spot used was 2–3 μm. A grating of 2400 lines/mm, providing a spectral resolution of better than 1.5 cm^{-1}, and a NEXT grating filter enabled good stray light rejection in the 15–550 cm^{-1} range. The spectra were acquired from different spots on the permingeatite grain in order to obtain spectra from different crystal orientations. Spectral manipulations were performed using the Omnic Spectral Tools software. Gaussian/Lorentzian profile functions of the band-shape were used to obtain decomposed band components of the spectra. The decomposition was based on the minimization of the difference in the observed and calculated profiles, until the squared correlation coefficient (r^2) was greater than 0.995.

Quantitative reflectance values were obtained with a Leica microscope (objective 100×) equipped with a J & M Tidas MSP 400 spectrophotometer. After careful levelling of the specimen and standard (Zeiss, WTiC), measurements were undertaken at intervals of 5 nm from 400 to 700 nm in air. Weak anisotropy made it difficult to orient the measured grains precisely at their extinction positions, but 14 grains were checked photometrically for maximal and minimal values.

Chemical Composition

According to previously published data on minerals of the luzonite-group, the types of substitution trends are very limited, except for those primarily involving Sb-Se-As. The only other element found to be entering the structures of the luzonite-group minerals in higher concentrations is Fe. We assume that the Fe is trivalent, similar to other minerals of the stannite group (Evstigneeva *et al*. 2003). Electron-microprobe data of permingeatite from Příbram (Table 1) indicates significant Se-S substitution, corresponding to the permingeatite-famatinite solid solution series, and minor contents of Fe, which does not clearly correlate with Cu, but Cu-Fe substitution, such as seen in stannite, is possible. The empirical formula (mean of 10 point analyses; on the basis of Sb + Cu + Fe + Se + S = 8 *apfu*) is $(Cu_{3.00}Fe_{0.04})_{\Sigma 3.04}Sb_{0.99}(Se_{3.74}S_{0.23})_{\Sigma 3.97}$. The relation between As and Sb *apfu* contents is shown in Figure 3. The observed Se-S substitution, according to the X-ray map, does not show any evolutionary trends or evidence of zoning.

Crystal Structure

The powder diffraction data for permingeatite from Příbram is presented in Table 2. The refined unit-cell parameters are *a* 5.6323(2) Å, *c* 11.2354(7) Å, with *V* 356.41(2) $Å^3$ (for space group $I\bar{4}2m$). The unit-cell parameters of permingeatite from Příbram are similar to those reported by Johan *et al.* (1971) for permingeatite from the type-locality Předbořice deposit (Table 3), and are smaller compared to those of synthetic perm-

ingeatite as reported by Pfitzner (1994). While there is an obvious Se-S substitution in permingeatite from Příbram, permingeatite from Předbořice is characterized by As-Sb substitution. Those data are consistent with the radii of the ions involved in the substitution in all cases. So it is obvious, according to our and published data, that As and S substitution in permingeatite leads to lower the cell parameters.

There are no mentions of the valence of Sb/As in minerals of the luzonite group in literature, but we presume that the valence of Sb/As in the permingeatite structure is 3+.

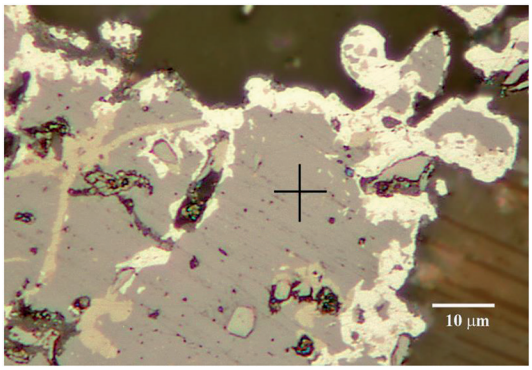

FIG. 2. Permingeatite grain in reflected light (grey with purple tint) with a rim of clausthalite (silver white) and thin purple veins of hakite.

RAMAN SPECTROSCOPY

In the structure of permingeatite (Pfitzner 1994) $SbSe_4$ and $CuSe_4$ tetrahedra are linked through shared corners (Fig. 4). In the primitive spectroscopic unit-cell three Cu, one Sb, and four Se atoms are localized (Table 4). The irreducible representations, representing the total number of the normal modes ($k = 0$), are $\Gamma_{red} = 2A_1(R) + A_2(-) + 2B_1(R) + 5B_2(IR,R) + 7E(IR,R)$, where IR and Raman activities of the modes are given in parentheses. The total number of degrees of freedom is half (24 instead of 48), because in $I\bar{4}2m$ symmetry the content of the primitive unit cell is half with regard to Z. One B_2 and one E mode are translations (corresponding to the three acoustic branches), and the A_2 (inactive)

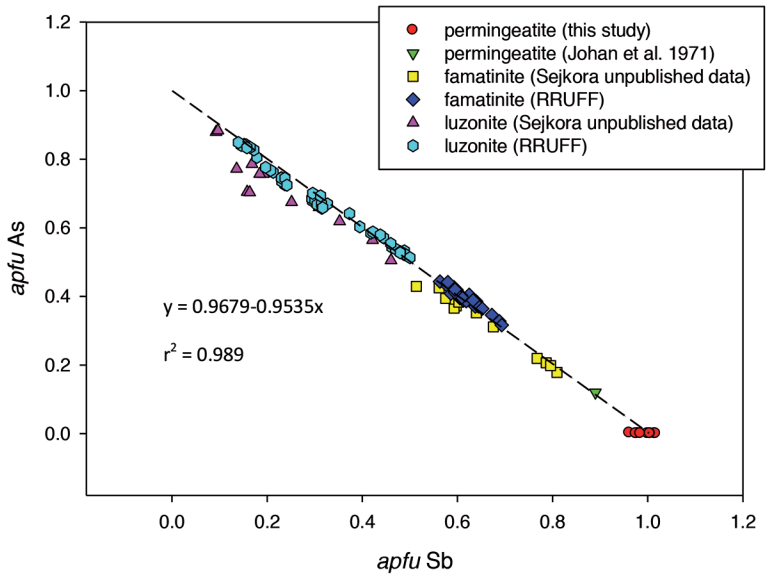

FIG. 3. Plot *apfu* Sb *versus apfu* As for permingeatite and the famatinite-luzonite series. Famatinite (Sejkora unpublished data) occurrences: Quiruvillca, La Libertad (Peru), Julcani, Huancavelica (Peru), Laurani, La Paz (Bolivia); famatinite (RRUFF) occurrences: Quiruvillca, La Libertad (Peru), Mohawk mine, Nevada (USA). Luzonite (Sejkora unpublished data) occurrences: Nevados de Famatina, La Rioja (Argentina), Castrovirreyna, Huanvelica (Peru); luzonite (RRUFF) occurrences: Mohawk mine, Nevada (USA) and Huranon, Pasco (Peru). Dashed line is the ideal correlation Sb:As = 1:1. Correlation relation for the whole set of data in the plot is $y = 0.9679 - 0.9535x$ and r^2 value for this relation and data is 0.989.

and one E mode are rotations. Thus, the number of the optical normal modes (without the acoustic ones) is $\Gamma_{vib} = 2A_1 + A_2 + 2B_1 + 4B_2 + 6E$, and as the E modes are doubly degenerated, the total number of degrees of freedom remains 21. In total, 14 Raman active vibrations can be detected, corresponding to vibrations of one $SbSe_4$ and one $CuSe_4$ tetrahedra. The orientations of the corresponding Raman tensors are also listed in Table 4.

Results of the band-component analysis of permingeatite, famatinite, and luzonite spectra (Fig. 5) are listed in Table 5, which gives the position of each vibration, its relative intensity, and the full width at half maximum (FWHM). The dominant feature of all permingeatite spectra measured from different spots on the mineral grain is the presence of intense vibration bands in the 250–150 cm^{-1} region. Lower frequency vibrations (below 100 cm^{-1}) should correspond to external modes, or translations of Cu and Sb atoms, and the middle-frequency bands to internal modes of the Se-tetrahedra (Fig. 6).

According to the literature (Nakamoto 1986), the main middle-frequency bands can be assigned to stretching vibrations of the $(Sb/Cu)Se_4$ tetrahedra. Copper atoms occupy two different sites in the lattice, forming two types of tetrahedra with different internal bond-lengths. Two different crystallographic Cu sites could also affect the number of external modes. The internal vibrations of isolated tetrahedra have been studied and measured for some compounds (Nakamoto 1986). In the case of the permingeatite structure, there is a network of linked tetrahedra which are not isolated; nevertheless, some comparison can be done. The normal tetrahedral vibrations in cubic symmetry can be divided into ν_1 (A_1, symmetric stretching), the doublet ν_2 (E, bending), and the triplets ν_3 (F_2, antisymmetric stretching) and ν_4 (F_2, antisymetric bending). In tetragonal symmetry, the doublet E splits into $A_1 + B_1$ and triplets F_2 split into $B_2 + E$ modes.

TABLE 1. ELECTRON MICROPROBE COMPOSITIONS FOR PERMINGEATITE FROM PŘÍBRAM

	Mean	Range	
wt.%		min	max
Cu	30.76	30.11	31.45
Sb	19.48	18.98	19.89
Fe	0.35	0.18	0.86
Se	47.62	45.84	48.60
S	1.17	0.83	2.26
Sum	99.51		
Cu*	2.999	2.926	3.059
Sb*	0.992	0.961	1.017
Fe*	0.039	0.020	0.095
Se*	3.737	3.546	3.830
S*	0.226	0.160	0.431

*based on 8 *apfu*. (*n* = 10)

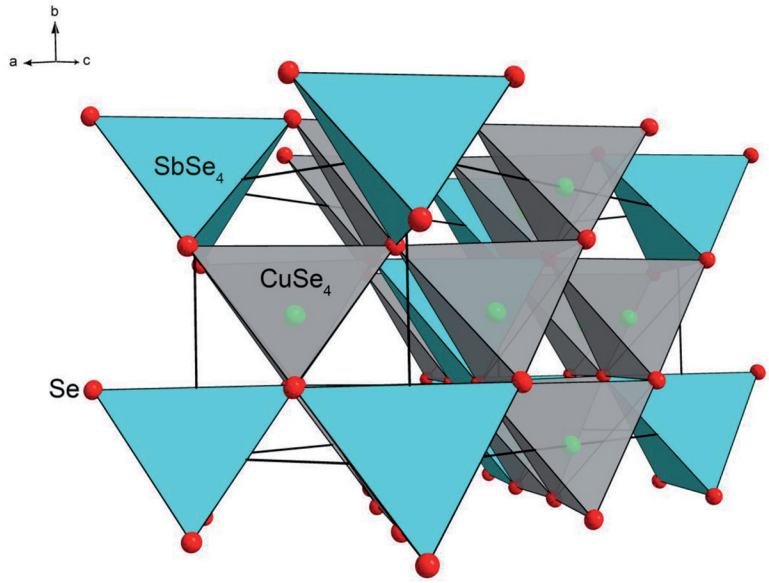

FIG. 4. Crystal structure of permingeatite (after Pfitzner 1994) in general projection, showing mutually interconnected $CuSe_4$ (grey) and $SbSe_4$ (azure) tetrahedra. Cu atoms are green, Se atoms are red. Unit-cell edges are outlined by a solid line.

From the literature it is known that famatinite spectra show the $(Sb/Cu)S_4$ modes ν_1 (A_1), ν_3 (B_2 + E), with frequencies around 366 and 380 cm^{-1} respectively (Nakamoto 1986). The replacement of S by Se in permingeatite should result in a substantial decrease of these frequencies [more than 100 cm^{-1}, as observed in $Nb(S/Se)_4$ or $Mo(S/Se)_4$ tetrahedra; see Nakamoto 1986]. This is confirmed in our spectra: $\nu_1(A_1)$ ~180, ν_3 (B_2 + E) ~220 cm^{-1}. The A_1 mode frequency should not depend much on the central atom; however, the antisymmetric (B_2 + E) vibration could be doubled due to the presence of Cu and Sb. As the Cu atom is almost half as light as Sb, we could expect higher frequencies for vibrations where Cu is involved. Further assignment concerning bending modes would be rather speculative due to the mixing of the normal modes in the case of non-isolated tetrahedra. Modes with A_1 symmetry arise from the symmetric stretching movement of the Se atoms. They have the highest Raman intensity in famatinite and luzonite (see Fig. 5), therefore the highest intensity band at ~185 cm^{-1} is attributable to this symmetric stretching vibration ν_1 (A_1) $(Cu/Sb)Se_4$. The band at ~130 cm^{-1} was ascribed to the bending mode ν_4 because of its lower intensity and lower frequency.

As we are not able to establish the crystal grain orientation in the matrix of the polished-section, we are not able to determine and assign the precise character (symmetry) of a given vibration mode. Therefore the assignments of the low frequency bands are only tentative. The external modes comprise vibrations of translational character B_2 + E (Raman active) and librations A_2 + E (where A_2 is only IR active). We can deduce that librations arise from movements of Se atoms coordinating a central atom represented by Cu or/and Sb. In Figure 5 several bands are observed; those at ~60 cm^{-1} and ~20 cm^{-1} correspond to emission lines of the laser, and the bands at the lowest wavenumbers should not be considered, due to the absorption edge of the NEXT filter below 20 cm^{-1}. Raman bands at 75, 78, 45, and 40 cm^{-1} should be connected with external modes — translations and librations. The presence and origin of the weak intensity band at 51 cm^{-1} is questionable, but could be assigned to the translational B_2 mode.

TABLE 2. X-RAY POWDER DIFFRACTION PATTERN OF PERMINGEATITE FROM PŘÍBRAM

h	*k*	*l*	d_{obs}	d_{calc}	I/I_0
0	1	1	5.033	5.035	6
1	1	0	3.985	3.983	1
1	1	2	3.248	3.249	100
0	1	3	3.121	3.119	8
0	2	2	2.5227	2.5175	1
1	2	1	2.4602	2.4578	2
1	1	4	2.2942	2.2954	<1
1	0	5	2.0887	2.0871	<1
2	0	4	1.9893	1.9887	22
0	0	6	1.8731	1.8726	<1
0	3	1	1.8543	1.8518	<1
3	1	2	1.6978	1.6978	10
1	3	4	1.5061	1.5042	<1
2	3	3	1.4438	1.4417	<1
0	4	0	1.4088	1.4081	1
3	1	6	1.2919	1.2905	2
2	4	4	1.1497	1.1492	2
3	3	6	1.0842	1.0830	<1

TABLE 3. THE REFINED UNIT-CELL PARAMETERS OF MEMBERS OF THE LUZONITE GROUP

	permingeatite this work	permingeatite Johan *et al.* (1971)	permingeatite Pfitzner (1994)	luzonite Downs (2006) RRUFF ID R060390	luzonite Downs (2006) RRUFF ID R060390
	$^{(1)}Cu_{3.00}(Sb_{0.99}Fe_{0.04})_{\Sigma 1.03}(Se_{3.74}S_{0.23})_{\Sigma 3.97}$	$Cu_{3.01}(Sb_{0.89}As_{0.12})_{\Sigma 1.01}Se_{3.98}$	Cu_3SbS_4	$Cu_{3.01}(As_{0.85}Sb_{0.15})_{\Sigma 1.00}S_4$	$^{(2)}Cu_{3.01}(As_{0.75}Sb_{0.28})_{\Sigma 1.03}S_4$
a [Å]	5.6323(2)	5.631(2)	5.6609(8)	5.339(6)	5.3193(9)
c [Å]	11.2354(7)	11.230(5)	11.280(5)	10.60(1)	10.543(2)
V [Å^3]	356.41(2)	356(1)	361.5	302.2(2)	298.3(1)
a/*c*	0.5013	0.504	0.4726	0.5037	0.5045

	luzonite-famatinite series Pfitzner & Bernert (2004)		famatinite Garin & Parthé (1972)	famatinite Pfitzner & Reiser (2001)	famatinite Downs (2006) RRUFF ID R110021
	$Cu_3(As_{0.33}Sb_{0.67})_{\Sigma 1.00}S_4$	$Cu_3(As_{0.736}Sb_{0.264})_{\Sigma 1.00}S_4$	Cu_3SbS_4	Cu_3SbS_4	$Cu_{3.02}(Sb_{0.53}As_{0.48})_{\Sigma 1.01}S_4$
a [Å]	5.353(1)	5.315(1)	5.294	5.391(1)	5.345(2)
c [Å]	10.652(2)	10.536(2)	10.653	10.764(1)	10.630(6)
V [Å^3]	305.2(1)	297.7(1)	298.5656	312.83(9)	303.7(1)
a/*c*	0.5025	0.5045	0.4969	0.5008	0.5028

(1) Mean from 10 electron microprobe analyses
(2) Mean of three electron microprobe analyses

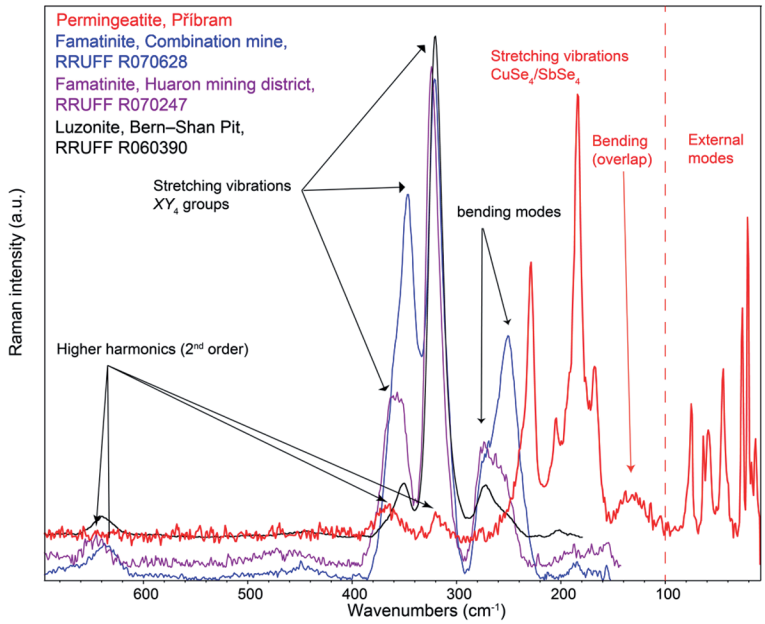

FIG. 5. Raman spectra of permingeatite (red), famatinite (blue, violet), and luzonite (black). Spectra are vertically offset for clarity.

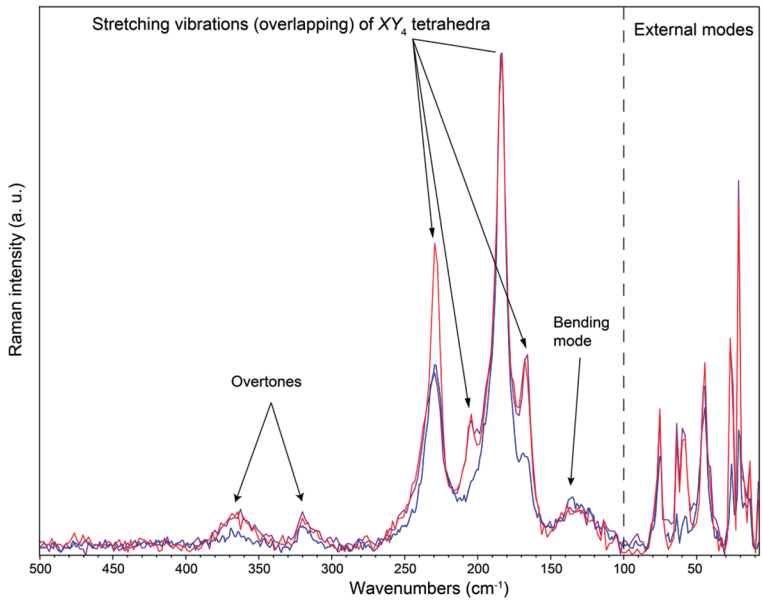

FIG. 6. Raman spectra of permingeatite acquired from three different spots (indicated by different line colors) within a grain in the polished section.

A comparison and comments on the spectra of famatinite and luzonite

As the crystal structures of luzonite, famatinite, and permingeatite are similar, we can expect similar Raman spectra, and that is what was observed (Figs. 5 and 6). The differences are only in the positions of the bands, because the energies of the X–Y (X = As/Sb; Y = S/Se) vibrations differ, according to Hook's rule. An intrinsic shift is observable comparing Sb-Se and Sb-S stretching modes, corresponding to permingeatite and famatinite, respectively.

Reflectance

Due to the relatively significant differences between the published reflectance curves for permingeatite from Předbořice (Johan *et al.* 1971, Picot & Johan 1982), the reflectance values were redetermined for permingeatite from Příbram (Table 6). The obtained data are close (Fig. 7) to the data published by Picot & Johan (1982). More significant differences were found when compared to the data published by Johan *et al.* (1971), particularly in the areas of 420–500 nm and about 640 nm (Fig. 8). It is possible that the material studied by Johan *et al.* (1971) contains inclusions of other minerals (*e.g.*, hakite, clausthalite, berzelianite) and their results were affected.

Conclusions

Permingeatite has recently been identified in material originating from the hydrothermal uranium deposit near Příbram by means of X-ray powder diffraction, reflectance, electron microprobe analysis, and Raman spectroscopy. Chemical compositions show greater Se-S substitution. No As, even trace amounts, was found by microprobe analysis in the permingeatite

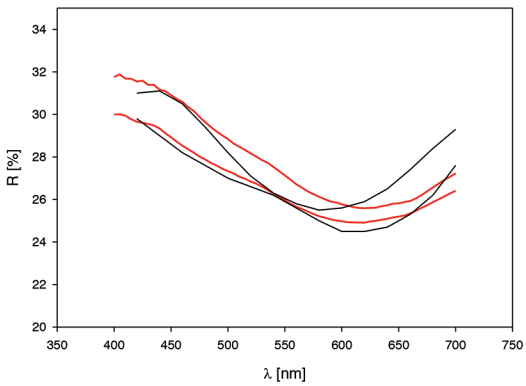

FIG. 7. Reflectance curves (R_{min}, R_{max}) for permingeatite from Příbram (red) in comparison with published data for permingeatite from Předbořice (Picot & Johan 1982).

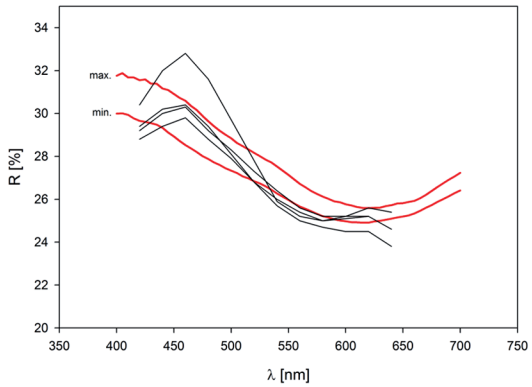

FIG. 8. Reflectance curves (R_{min}, R_{max}) for permingeatite from Příbram (red) in comparison with published data for permingeatite from Předbořice (Johan *et al.* 1971).

TABLE 4. FACTOR GROUP ANALYSIS FOR PERMINGEATITE, Cu_3SbSe_4 (SPACE GROUP NO. 121, $I\bar{4}2m$)

Atom	Wyckoff	Site-symmetry	Γ_{red} G_F
Sb	*a*(2)	$\bar{4}2m$	B_2+E
Cu	*b*(2)	$\bar{4}2m$	B_2+E
Cu	*d*(4)	$\bar{4}$	B_1+B_2+2E
Se	*i*(8)	*m*	$2A_1$+A_2+B_1+$2B_2$+3E
TOTAL		– (B_2 + E)	= $2A_1$ + A_2 + $2B_1$ + $4B_2$ + 6E
	IR	RA	
A_1		a_{xx}+a_{yy}, a_{zz}	
A_2	R_z		
B_1		a_{xx}–a_{yy}	
B_2	T_z	a^z_{xy}	
E	(T_x, T_y); (R_x, R_y)	(a^y_{xz}, a^x_{yz})	

TABLE 5. BAND-COMPONENTS OF THE RAMAN SPECTRA OF STUDIED MINERALS

Perm[1]	Perm[2]	Perm[3]	Fam[R070247]	Fam[R070628]	Luz[R060390]
position / relative intensity / FWHM (cm^{-1}/ % / cm^{-1})					
			695/4/37		
					683/1/21
				669/2/16	
			676/1/8		
			646/9/26		
				636/6/21	**639**/5/25
			585/1/73	**584**/1/21	**590**/<1/32
				492/1/32	**495**/<1/40
					460/1/23
			476/4/61		
			448/2/40	**446**/3/16	**443**/1/16
					427/1/17
				395/1/7	
374/5/16	**379**/2/10		**379**/6/9		
366/4/10	**367**/3/10	**368**/4/18	**365**/43/16		**362**/4/14
357/4/15	**358**/2/8		**357**/2/1	**359**/41/19	
		349/2/18	**352**/46/17	**346**/61/12	**351**/10/12
				334/25/8	
			325/100/11	**321**/100/13	**322**/100/12
318/5/12	**316**/3/7	**319**/6/12	**319**/87/19		**315**/41/13
				309/26/10	**305**/7/14
				302/8/7	
276/2/3			**275**/36/15	**277**/15/11	**272**/11/17
				269/15/9	
			263/5/3	**261**/20/11	
251/4/14	**252**/2/10		**257**/32/23		**254**/5/19
		246/4/19		**249**/44/15	
237/19/12	**240**/5/12			**237**/11/11	
229/60/7	**229**/41/13	**230**/46/14			
			222/4/2		
214/7/13	**215**/5/10	**215**/4/8			
205/20/8	**203**/8/12	**204**/7/13			**202**/1/9
193/26/12	**191**/29/13	**192**/12/10		**190**/1/5	
184/100/7	**184**/100/6	**184**/100/6		**184**/3/6	
		183*/31/25			
176/20/8	**177**/19/9				
167/36/8	**167**/17/9	**166**/12/7			
159/1/4	**156**/3/7				
	147/2/8				
140/4/12					
	136/10/12	**136**/9/15			
127/7/22	**125**/7/12	**124**/6/17			
	113/3/9				
	91/3/3				
	80/3/2	**80**/3/4			
78/10/4	**77**/9/4				
75/32/3	**75**/28/3	**75**/24/4			
	70/4/4				
63/21/2	**63**/23/2				
59/26/5	**59**/29/5				
51/3/2	**51**/6/6				
45/40/4	**45**/33/5	**45**/43/6			
40/9/3	**40**/14/3				
	36/5/1				
26/60/2	**26**/65/3	**26**/18/2			
21/90/2	**21**/88/2	**21**/28/2			
17/14/2	**17**/10/3				
14/23/3	**14**/24/3				

TABLE 6. REFLECTANCE DATA FOR PERMINGEATITE, MEASURED IN AIR

λ [nm]	Příbram this paper		Předbořice Picot & Johan (1982)		Předbořice Johan *et al.* (1971)			
	$R_{min.}$	$R_{max.}$	$R_{min.}$	$R_{max.}$	$R_{min.}$	$R_{max.}$	$R_{min.}$	$R_{max.}$
400	30.0	31.8	-	-	-	-	-	-
420	29.7	31.5	29.8	31.0	29.4	30.4	28.8	29.2
440	29.3	31.2	29.0	31.1	30.2	32.0	29.4	30.0
460	28.5	30.6	28.2	30.5	30.4	32.8	29.8	30.3
480	27.9	29.6	27.6	29.4	29.4	31.6	28.8	29.2
500	27.3	28.8	27.0	28.2	28.1	29.7	27.9	28.3
520	26.8	28.2	26.6	27.1	26.8	27.8	26.8	27.3
540	26.3	27.5	26.2	26.3	25.7	25.9	26.0	26.4
560	25.7	26.7	25.6	25.8	25.0	25.2	25.4	25.6
580	25.2	26.1	25.0	25.5	24.7	25.0	25.0	25.2
600	25.0	25.8	24.5	25.6	24.5	25.2	25.1	25.2
620	24.9	25.6	24.5	25.9	24.5	25.6	25.2	25.2
640	25.1	25.7	24.7	26.5	23.8	25.4	24.6	24.6
660	25.3	25.9	25.3	27.4	-	-	-	-
680	25.9	26.6	26.2	28.4	-	-	-	-
700	26.4	27.2	27.6	29.3	-	-	-	-

studied. This is probably due to the fact that, in the calcite-uraninite stage, nearly all of the As is in other mineral phases, such as native arsenic, arsenolamprite, rare löllingite, and arsenopyrite, which are older than permingeatite in the paragenetic sequence.

Comparison of the Raman spectra of the luzonite mineral group shows obvious shifts in the wavenumbers of the stretching vibrations corresponding to the appropriate *X–Y* bonding-pair (where *X* = As/Sb; *Y* = S/Se).

The reflectance of permingeatite from Příbram is similar to the data published by Picot & Johan (1982), but there are significant differences from the original data published by Johan *et al.* (1971), which could be evidence of inclusions of other ore minerals in the type material.

Permingeatite was formed together with other known selenides from the Příbram uranium and base-metal deposit in the calcite-uraninite stage at relatively low temperatures, about 140–80 °C and from low-salinity solutions, probably of meteoric origin (Žák & Dobeš 1991). The presence of umangite in association with permingeatite supports the temperature of origin of the studied mineral assemblage being under 112 °C (Simon & Essene 1996).

Acknowledgements

We thank Radek Škoda (Masaryk University, Brno) for his cooperation during the analytical work. Thorough reviews by Sherif Kharbish, Andrew McDonald, and two anonymous referees, as well as the editorial care of Frédéric Hatert, are highly appreciated. This work was financially supported by Ministry of Education of the Czech Republic (MSM 0021620855) and by the grant DKRVO 2013/02, 00023272 of the Ministry of Culture of the Czech Republic. The Premium Academiae grant of the ASCR, v.v.i. and the post-doctoral grant 13-31276P (GACR) are acknowledged for providing financial support to JP.

References

Coelho, A.A. & Cheary, R.W. (1997) *X-ray Line Profile Fitting Program, XFIT*. School of Physical Sciences, University of Technology, Sydney, NSW, Australia.

Downs, R.T. (2006) The RRUFF Project: an integrated study of the chemistry, crystallography, Raman and infrared spectroscopy of minerals. *19th General Meeting of the International Mineralogical Association, Kobe, Japan, Program and Abstracts*, 3–13.

Dymkov, J.M. (1985) Selenidy nasturan-karbonatnych žil. *In* Paragenezis mineralov uranonosnych žil. Nedra, Moscow, Russia (153–162).

Ettler, V., Sejkora, J., Drahota, P., Litochleb, J., Pauliš, P., Zeman, J., Novák, M., & Pašava, J. (2010) Příbram and Kutná Hora mining districts—from historical mining to recent environmental impact. *Acta Mineralogica-Petrographica Field Guide Series* **7**, 1–23.

Evstigneeva, T.L., Rusakov, V.S., & Kabalov, Y.K. (2003) Isomorphism in the minerals of the stannite family. *New Data on Minerals* **38**, 65–70.

Gaines, R.V. (1957) Luzonite, famatinite and some related minerals. *American Mineralogist* **42**, 766–779.

GARIN, J. & PARTHÉ E. (1972) The crystal structure of Cu_3PSe_4 and other ternary normal tetrahedral structure compounds with composition 1_356_4. *Acta Crystallographica* **B28**, 3672.

HOLLAND, T.J.B. & REDFERN, S.A.T. (1997) Unit cell refinement from powder diffraction data: the use of regression diagnostics. *Mineralogical Magazine* **61**, 65–77.

JOHAN, J., PICOT, P., & PIERROT, R. (1971) La permingeatite Cu_3SbSe_4, un noveau minéral du groupe de la luzonite. *Bulletin de la Société française de Minéralogie* **94**, 162–165.

LAUGIER, J. & BOCHU, B. (2004) *Celref, version 3*. Domaine Universitaire, Grenoble, France.

LEGIERSKI, J. (1973) Model ages and isotopic composition of ore leads of the Bohemian Massif. *Krystalinikum* **3**, 87–98.

LITOCHLEB, J., SEJKORA, J., & ŠREIN, V. (2004) Selenidy z ložiska Bytíz (Příbramský uran-polymetalický revír). *Bulletin Mineralogicko-Petrologického Oddělení Národního Muzea v Praze* **12**, 113–123.

MARUMO, F. & NOWACKI, W. (1967) A refinement of the crystal structure of luzonite, Cu_3AsS_4. *Zeitschrift für Kristallographie* **124**, 1–8.

NAKAMOTO, K. (1986) *Infrared and Raman spectra of inorganic and coordination compounds*. John Wiley and Sons, New York, United States.

PANALYTICAL, B.V. (2003) *X'Pert High Score*. Almelo. Netherlands.

PAULING, W. & WEINBAUM, S. (1934) The crystal structure of enargite, Cu_3AsS_4. *Zeitschrift für Kristallographie* **88**, 48–53.

PFITZNER, A. (1994) Crystal structure of tricopper tetraselenoantimonate (V), Cu_3SbSe_4. *Zeitschrift für Kristallographie* **209**, 685.

PFITZNER, A. & REISER, S. (2002) Refinement of the crystal structures of Cu_3PS_4 and Cu_3SbS_4 and a comment on normal tetrahedral structures. *Zeitschrift für Kristallographie* **217**, 51–54.

PFITZNER, A. & BERNERT, T. (2004) The system Cu_3AsS_4–Cu_3SbS_4 and investigations on normal tetrahedral structures. *Zeitschrift für Kristallographie* **219**, 20–26.

PICOT, P. & JOHAN, Z. (1982) *Atlas of ore minerals*. Bureau de Recherches Géologiques et Minières, Paris, France and Elsevier Scientific Publishing Company, Amsterdam, Netherlands.

PÓSFAI, M. & BUSECK, P.R. (1998) Relationships between microstructure and composition in enargite and luzonite. *American Mineralogist* **83(3–4)**, 373–382.

POUCHOU, J.L. & PICHOIR, F. (1985) "PAP" procedure for improved quantitative microanalysis. *In* Microbeam Analysis (J.T. Armstrong, ed.). San Francisco Press, San Francisco, California, United States (104–106).

RŮŽIČKA, J. (1986) *Nerosty příbramského uranového ložiska*. Kamenná, Vydal *Komitét Symposia Hornická Příbram* ve *vědě* a technice, 244pp.

SEJKORA, J., ŠKODA, R., & PAULIŠ, P. (2006) Selenium mineralization of the uranium deposit Zálesí, the Rychlebské Hory Mts., Czech Republic. *Mineralogia Polonica* **28**, 196–198.

SEJKORA, J., MAKOVICKY, E., TOPA, D., PUTZ, H., ZAGLER, G., & PLÁŠIL, J. (2011) Litochlebite, $Ag_2PbBi_4Se_8$, a new selenide mineral species from Zálesí, Czech Republic: description and crystal structure. *Canadian Mineralogist* **49**, 639–650.

SIMON, G. & ESSENE, E.J. (1996) Phase relations among Selenides, Sulphides, Tellurides, and Oxides: I. Thermodynamic Properties and Calculated Equilibria. *Economic Geology* **91**, 1183–1208.

STELZNER, A. (1873) Mineralogische beobachtungen im gebiete der Argentinischen Republik. *Mineralogische Mittheilungen* **4**, 219–254.

ŠKÁCHA, P., GOLIÁŠ, V., SEJKORA, J., PLÁŠIL, J., STRNAD, L., ŠKODA, R., & JEŽEK, J. (2009a) Compositional trends in hakite, possible discrepancies from ideal structure. *Acta Mineralogica-Petrographica Abstract Series* **6**, 725.

ŠKÁCHA, P., SEJKORA, J., LITOCHLEB, J., & HOFMAN, P. (2009b) Výskyt cuprostibitu v příbramském uran-polymetalickém revíru (šachta 16, Příbram - Háje), Česká republika. *Bulletin Mineralogicko-Petrologického Oddělení Národního Muzea v Praze* **17(1)**, 73–78.

ŠKÁCHA, P., VLČEK, V., SEJKORA, J., PLÁŠIL, J., & GOLIÁŠ, V. (2010) Compositional trends in hakite, possible discrepancies from ideal structure. *Acta Mineralogica-Petrographica Abstract Series* **6**, 725.

TOPA, D., MAKOVICKY, E., SEJKORA, J., & DITTRICH, H. (2010) The crystal structure of watkinsonite, $Cu_2PbBi_4Se_8$, from the Zálesí uranium deposit, Czech Republic. *Canadian Mineralogist* **48**, 1109–1118.

WEISBACH, A. (1874) Luzonit. *In* Mineralogische Mittheilungen (G. Tschermak, ed.). Wilhelm Braumüller, Vienna, Austria (257–258).

ŽÁK, K. & DOBEŠ, P. (1991) Stable isotopes and fluid inclusions in hydrothermal deposits: the Příbram ore region. *Rozpravy Československá akademie věd Řada Matematických a Přírodních Věd* **101**, 1–109.

Received June 28, 2013. Revised manuscript accepted February 24, 2014.